PROCEEDINGS OF SCIENCE

The Extragalactic Background Light: Constraints from TeV Blazar Observations

Elisa Pueschel[*†]
Deutsches Elektronen-Synchrotron (DESY)
Platanenalle 6, D-15738 Zeuthen, Germany
E-mail: elisa.pueschel@desy.de

Ground-based imaging atmospheric-Cherenkov telescope arrays such as VERITAS, H.E.S.S. and MAGIC have collected deep exposures on hard-spectrum blazars located at a range of redshifts, in addition to shorter exposures during periods of high source activity. These datasets can be used to characterize the intensity spectrum of the extragalactic background light (EBL), as interactions of γ-rays emitted by the sources with EBL photons impact the observed photon spectra of distant blazars. We present an overview of EBL constraints and measurements derived from observations made by these instruments.

35th International Cosmic Ray Conference — ICRC2017
10–20 July, 2017
Bexco, Busan, Korea

[*]Speaker.
[†]full author list for VERITAS results at https://veritas.sao.arizona.edu/

PoS(ICRC2017)1107

1. Introduction

The extragalactic background light (EBL) refers to an ambient photon field produced by all radiation processes and re-radiation after absorption by dust, beginning with the epoch of recombination (for a review, see [1]). As such, it encodes information about the formation and evolution of stars and galaxies, as well as active galactic nuclei. While these processes can be studied directly via observations of the systems, radiation sources that cannot be observed directly could potentially also be reflected in the energy distribution and intensity of the EBL. For instance, diffuse or as-yet unresolved sources could increase the EBL density, as could radiation from dark matter annihilation or decay processes, or exotic processes early in the universe's evolution.

The spectral energy distribution (SED) of the EBL is predicted to contain two peaks: the cosmic optical background (COB) at λ_{EBL} = 0.1-10 μm, and the cosmic infrared background (CIB) at λ_{EBL} = 10-100 μm. A schematic showing the EBL intensity distribution as a function of wavelength/frequency of the EBL photons is shown in Figure 1 [2]. The COB is primarily due to direct radiation from stars and galaxies, whereas the absorption and re-radiation of light by dust particles is responsible for the CIB. The EBL tracks galactic and stellar evolution, and consequently varies with redshift. The schematic shown in Fig. 1 represents the distribution at z=0.

The EBL designates just one segment of the diffuse photon field present in the universe: radio, ultraviolet, X-ray, and γ-ray backgrounds are also present, as well as the cosmic microwave background (CMB). The EBL is indeed intimately connected with diffuse photon fields at other wavelengths (radio and X-ray), as well as the diffuse neutrino background. This is a reflection of the fact that the same physical processes produce a variety of types of radiation: for instance, light from main sequence stars is a major contributor the COB, and the neutrinos produced when the same stars undergo supernovae at the end of their life cycles contribute to the diffuse neutrino background. Consequently, EBL measurements are important for evaluating the overall consistency of our picture of diffuse radiation fields.

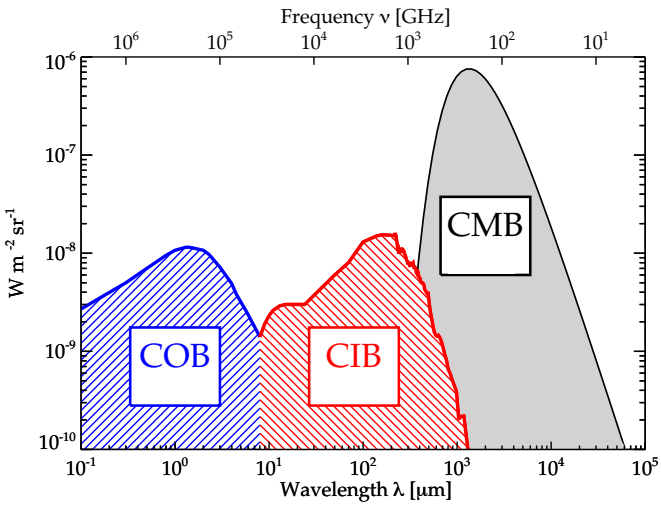

Figure 1: A schematic of the EBL intensity as a function of wavelength/frequency. Figure adapted from [2].

2. Modeling the EBL

A variety of approaches have been taken to modeling the EBL intensity and spectrum (for examples of recent models, see [3, 4, 5, 6, 7]). The methods used to derive the most commonly used models can be divided into three classes: background evolution (e.g. [3, 4, 7]), forward evolution (e.g. [6]), and semi-analytical models (e.g. [5]). A detailed description of these three approaches can be found in [8]. To briefly summarize, all models make a calculation of the luminosity density $\mathscr{L}_\nu(\nu,z)$. This function is then integrated (from $z=0$ to a maximum redshift z_{max} at which galaxy formation is assumed to begin) to derive the EBL. Backward evolution models start with the local luminosity density $\mathscr{L}_\nu(\nu,0)$ and extend it to higher redshifts using empirical parameterizations of galaxy evolution. Forward evolution models, on the other hand, start with initial stellar populations and an assumed cosmic star formation rate, and model stellar and galactic evolution processes from z_{max} to z=0. These models taken into account the evolving dust distribution and composition with either parameterizations of the evolution or radiative transfer models. Semi-analytical models rely on modeling of structure formation in a ΛCDM universe to predict the properties and evolution of galaxies and galaxy clusters, which is again translated into a prediction of $\mathscr{L}_\nu(\nu,z)$. As opposed to forward evolution models, which assume a fixed star formation rate, semi-analytical models take into account galactic interactions and morphological evolution of galaxies which affect the star formation rate.

All models can be compared to observed galaxy counts at different redshifts. Forward evolution and semi-analytical models incorporate more information about physical processes than backward evolution models, resulting in many tunable parameters describing the evolution of galaxies and absorption by dust. In spite of the different approaches of the models, predictions for the COB intensity are fairly consistent for recent models (see Fig. 9 of [1] for a comparison). Predictions for CIB intensity can differ by several factors, largely due to the complications of modeling the dust distribution and evolution.

3. Direct measurements and galaxy counts

Upper and lower limits on the EBL have been provided by direct measurements and estimations based on galaxy counts, respectively. The limits are summarized with references in [1], and are plotted in Fig. 2. Direct measurements are, as the name implies, measurements of the sky brightness far from the galactic plane, conducted above Earth's atmosphere. Their accuracy hinges on the correct subtraction of source contamination (e.g. light from stars) and diffuse contamination from the zodiacal light, as well as instrumental calibration. Given the challenges of the measurements, the results are generally regarded as upper limits on the EBL intensity. Recent measurements have been provided by the *COBE*, FIRAS, and DIRBE instruments.

Robust lower limits on the EBL are set by summing the light from resolved galaxies, using galaxy counts in magnitude bands. These measurements have benefited from deeper surveys and stacking analyses, both of which reduce the number of unresolved sources. While the EBL may indeed be fully resolved by these measurements, they are insensitive to light emitted by sources other than galaxies, such as exotic processes or truly diffuse emission.

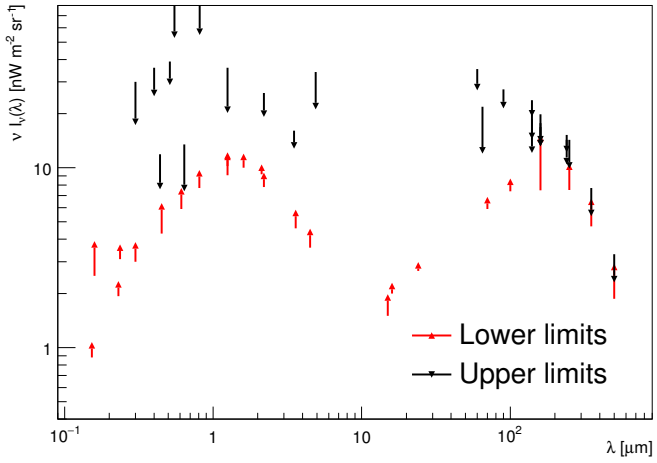

Figure 2: Upper and lower limits on the EBL from direct measurements (black downward arrows) and estimations based on galaxy counts (red upward arrows).

4. The γ-ray opacity of the universe

In light of the limitations of both direct measurements and estimates of the EBL with galaxy counts, there is clearly motivation for additional measurements with independent methods. Observations of distant γ-ray sources provides such a complementary approach. Photons of energy 100 GeV to 100 TeV interact with COB and CIB photons via pair production of electrons and positrons, resulting in an energy and redshift attenuation of the intrinsic γ-ray emission. The threshold for pair production is given by

$$\varepsilon_{th}(E_\gamma, cos\theta, z) = \frac{2(m_e c^2)^2}{E_\gamma(1-cos\theta)(1+z)} \tag{4.1}$$

where θ defines the angle between the primary and EBL photon, and the factor $(1+z)$ accounts for the decrease in the initial photon energy due to redshift. Once above threshold, the cross section for pair production depends on the Thompson cross section and the energies of the photons [9].

The attenuation of a γ-ray emitting source's initial photon flux due to pair production interactions as the photons travel to the observer can be quantified as an optical depth τ, such that the observed photon flux Φ_{obs} and initial emitted photon flux at a source Φ_0 are related by $\Phi_{obs} = \Phi_{int} e^{-\tau}$. Deriving τ requires integration of the pair production cross section and the number density of EBL photons over energy, as well as the distance between the source and the observer and the angles between the EBL and primary photons. The distance element is given by

$$\frac{dl}{dt} = \frac{c}{H_0} \frac{1}{1+z} \frac{1}{\sqrt{\Omega_\Lambda + \Omega_M (1+z)^3}} \tag{4.2}$$

where H_0 is the Hubble constant and Ω_Λ and Ω_M are the dark energy and matter densities, respectively. The number density of EBL photons depends on both the EBL photon energy and the redshift. This quantity is the kernel of EBL model predictions: the density of EBL photons as a function of energy, and the evolution of this quantity with redshift.

While the full details are not covered here, it is worth mentioning that due to the dependence of the pair production cross section on the emitted and EBL photons, it can be derived that high energy (10 -100 TeV) photons primarily interact with EBL photons of the CIB, whereas lower energy (100 GeV - 10 TeV) photons probe the COB. Consequently, improved measurements of the CIB, for which model predictions show more of a spread than for the CIB, must reply on observations of γ-ray sources that emit photons to tens of TeV.

Fig. 3 shows the attenuation $e^{-\tau}$ versus the primary γ-ray energy for the EBL model of [5] at a variety of source redshifts. The attenuation increases dramatically with energy and redshift. The relation between the attenuation, energy, and distance can also be expressed as the *cosmic γ-ray horizon*, the energy and redshift for which τ=1.

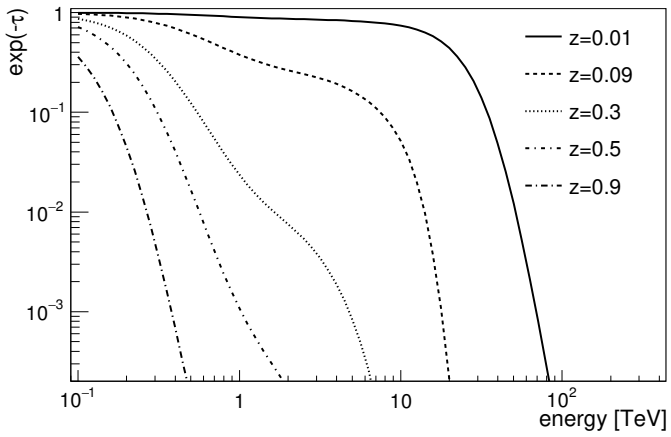

Figure 3: The attenuation $e^{-\tau}$ versus the primary γ-ray energy for the EBL model of [5].

5. EBL imprint on blazar spectra

Active galactic nuclei, particularly blazars, present an appealing source class for the study of the EBL. Briefly described, blazars feature a relativistic jet, powered by accretion onto a supermassive black hole at the center of the galaxy. The angle of the jet is aligned with the observer's line of sight. Observations of blazars in the local universe demonstrate that some blazars emit photons from thermal energies to tens of TeV. Furthermore, blazars are detected at cosmological distances: to $z \sim 1$ at very high energies (VHE; E>100 GeV) and $z \sim 3$ at high energies (HE; 10 MeV<E<100 GeV).

Blazar photon spectra are consequently strongly affected by EBL attenuation at high energies and high redshifts. Accurate characterization of the EBL is necessary to relate an observed photon spectrum to the intrinsic spectrum at the source. Taken in the opposition direction, after making some assumption about the intrinsic photon spectrum, blazar spectral observations can be used to characterize the EBL. The broad energy range of emitted γ-rays and distribution to high redshifts allow blazar spectral observations to probe a range of optical depths. As suggested above, observations at HE can be used to constrain the COB (particularly below $\lambda = 1\mu$), while VHE observations can probe the COB and the high-energy side CIB peak.

The observed photon spectrum can be expressed as

$$\left(\frac{dN}{dE}\right)_{obs} = \left(\frac{dN}{dE}\right)_{int} e^{-\tau}. \tag{5.1}$$

As one does not have access to the intrinsic spectra, some set of assumptions must be made about their form. In general, it is assumed that the spectra cannot be convex (i.e. flux increasing with energy), but instead can be described by a power law ($dN/dE \propto E^{-\Gamma}$), or a concave curved shape such as a power law with exponential cutoff or a log parabola. The shape of the VHE spectrum can also be constrained to extend smoothly from the observed HE spectrum, which for low redshift sources is minimally affected by EBL attenuation. However, the possibility remains that an intrinsic source cutoff can be misattributed to EBL attenuation, resulting in an overestimate of τ. On the other hand, assuming that a source cutoff must be present in the observed energy range can similarly result in an underestimate of τ. Sensitivity to source-specific effects can be reduced by studying a large sample of blazars at a range of redshifts. Spectral cutoffs or curvature due to EBL attenuation are expected to evolve with redshift (moving to lower energies with increasing z), whereas intrinsic cutoffs do not.

A further confounding factor is the flux and spectral variability of blazars. Blazars have been observed to undergo changes in flux at timescales from minutes to years, sometimes by orders of magnitude. This can be accompanied by changes in the spectral index Γ. This can render invalid the use of a time-averaged photon spectrum as combining multiple spectral and flux states can artificially produce the appearance of upward or downward spectral curvature. Furthermore, rapid variability complicates the extrapolation of HE spectra to the VHE range, due to the different flux sensitivities of the instruments covering the two energy ranges.

A number of constraints and measurements have also been made using HE and VHE spectral measurements, for example [10], [11], [12] and [13] (several of these will be discussed further in this proceeding). Two approaches are common, which we denote as “model-dependent" ([10], [12]) and “model-independent" ([11], [13]). In the model-dependent case, values of τ appropriate to the redshift of the source and the energies of its spectral points are taken from an EBL model. The observed spectrum is then fit with the function

$$\left(\frac{dN}{dE}\right)_{obs} = \left(\frac{dN}{dE}\right)_{int} e^{-\alpha\tau}. \tag{5.2}$$

where α is a scale factor that is fit simultaneously with the spectral parameters. Reliance on the shape of an EBL model’s SED can be removed by separating it into wavelength ranges, and allowing the scale factor α to float independently in these ranges. Alternately, an ensemble of shapes representing the EBL spectral energy distribution at z=0 can be produced, and used to calculate τ as a function of energy. Redshift evolution of the EBL can be handled empirically via a factor f_{evo} that modifies the scaling of the EBL number density with redshift, making it possible to derive the EBL SED at a source redshift from its shape at z=0. The factor f_{evo} is selected such that the EBL evolution with redshift of a model is approximated. A full discussion can be found in [14].

It should be noted that for both the model-dependent and model-independent approaches, the EBL evolution with redshift is either taken directly from or fixed to approximate the predictions of an EBL model. Thus, some dependence on EBL model predictions is present in both cases.

6. γ-ray observations

The currently-operating γ-ray observatories cover the energy range from 100 MeV to $\sim$100 TeV. The Large Area Telescope (LAT) onboard the *Fermi* satellite, covers the HE range with sensitivity to photons between 100 MeV to >300 GeV. Photons are reconstructed from pair-conversion events in the detector. The LAT benefits from a large duty cycle, and is able to observe the entire sky in $\sim$3 hours.

In the VHE range, the most sensitive instruments are Imaging Atmospheric Cherenkov Telescopes (IACTs), which image air showers induced by VHE γ-rays impinging on Earth's atmosphere. The currently operating instruments are VERITAS [16] and MAGIC [17] in the northern hemisphere and H.E.S.S. [18] in the southern hemisphere. The sensitive energy range of the IACTs extends from $\sim$100 GeV to >30 TeV. IACTs make pointed observations with a limited field of view, and have a limited duty cycle, requiring good weather and low moonlight. Typical energy resolution for IACTs is between 15% and 25%, depending on the energy.

The future Cherenkov Telescope Array (CTA) [19] will advance significantly beyond the capabilities of existing instruments. CTA will include 118 telescope of three sizes, located on both northern and southern sites. The sensitive energy range of CTA will range from $\sim$20 GeV to 300 TeV, with a factor of $\sim$10 better sensitivity than the currently operating instruments.

7. Recent EBL measurements and constraints

An exhaustive survey of the current literature is beyond the scope of this proceeding. We focus instead on the EBL measurements that were presented for the first time at this conference. However, the reader is referred to a number of important results. In the HE range, these include the first *Fermi*-LAT detection of the EBL [10], and single-instrument EBL studies using the spectral evolution with energy of blazars in the second and third *Fermi*-LAT hard source catalogues [20, 21].

In the VHE range, [22] takes an alternate approach to the methods discussed above by predicting the intrinsic VHE spectra of 15 blazar based on synchrotron self-Compton models using their lower-energy (radio to HE) spectra, and comparing the intrinsic spectra absorbed with the EBL model of [3] against the observed VHE spectra. The measurement of [13] incorporates a remarkable dataset of 30 blazars and 86 spectra from different IACTs, resulting in an 11σ detection of the EBL and ruling out 4 of the then-mainstream EBL models. Also interesting was the detection of the distant blazar PKS 1441+25 by MAGIC and VERITAS [23]. At redshift z=0.939, this is one of the most distant blazars detected to date, and it was used to set limits on the EBL in the near-ultraviolet to near-infrared range that are competitive with multi-source constraints. Looking forward, CTA projections for the measurement of the EBL are given in [24].

7.1 VERITAS

We discuss the VERITAS EBL results in detail, as they do not appear in another proceeding or publication. A list of the sources included in the study is shown in Table 1. All of the objects studied were high-frequency-peaked BL Lac (HBL) objects. The sample was selected to cover a broad redshift range, and to include sources with hard spectral indices in the HE range (and consequently

Target	Source Class	Redshift	Exposure [hr]	Observed Spectrum
1ES 2344+514	HBL	0.044	47	curved
H1426+428	HBL	0.129	81	curved
1ES 0229+200	HBL	0.14	140	power law
1ES 1218+308	HBL	0.182	159	power law
1ES 1011+496	HBL	0.212	37	power law
MS 1221.8+2452	HBL	0.218	2	power law
1ES 0414+009	HBL	0.287	108	power law
PKS 1424+240	HBL	0.604	178	power law

Table 1: Summary of source properties and collected exposures for blazars included in the VERITAS EBL analysis.

predicted VHE spectra extending to high energies, assuming a power-law extrapolation from the HE range).

The data presented here were collected between the start of VERITAS operations in 2007 and the summer of 2016. The exposure times for each object are given in Table 1. In the case of MS 1221.8+2452, the source was only detectable during periods of high activity; consequently the datasets are substantially smaller than for brighter sources. The data were reduced with the standard VERITAS analysis pipelines [28, 29]. All sources are detected at significances above 5σ (and at much higher significances for brighter sources and longer exposures), making it possible to reconstruct photon spectra.

As discussed above, flux variability is a known property of blazars. With the exception of 1ES 0414+009, all sources studied show evidence for flux variability, or a clearly detected flare in the cases of 1ES 2344+514, 1ES 1011+496, MS 1221.8+2452, and PKS 1424+240. Spectral variability could potentially warp the time-averaged spectra: combining hard and soft spectral states would introduce a spectral break if one component dominates at high or low energies. The impact on the spectra was studied by dividing the datasets into high and low state, or into flare and non-flare datasets. No significant variability in the fitted spectral indices was found for any of the sources. Thus the time-averaged spectra were used in the following analysis.

Table 1 lists the shapes of the observed spectra. The observed spectra were fit with a simple χ^2 fit. Most of the observed spectra were well described by a power law; however, several required a curved model—either a power law with an exponential cutoff, or a log parabola—to achieve an acceptable fit (p-value$>$0.05).

We attempted to minimize assumptions about the shape of the EBL SED and the intrinsic source spectra in using the VERITAS-measured photon spectra to determine the EBL. The following procedure was used:

- A set of 480,000 generic EBL SED shapes was generated by drawing second order splines through a set of 12 points in λ_{EBL}/EBL intensity space (λ_{EBL}=0.18-100 μm at 12 fixed values of λ_{EBL}, EBL intensity at 12 randomly selected values between 1 and 50 nW m^{-2} sr^{-1}). Example shapes are shown in Figure 4. Constraints from galaxy counts and direct measurements were not considered; at each λ_{EBL}, a random number was thrown according to a flat distribution in *log* space. The intensity range was only restricted to avoid more than doubling

or halving the EBL intensity from one λ_{EBL} point to the next. This results in a non-flat initial intensity distribution at each λ_{EBL}, which is compensated for with weights.

- The value of $\tau(E,z)$ was calculated for energies from 100 GeV to 20 TeV and redshifts from z=0.03 to 1. This was done for a grid of 24 points in energy and 17 points in redshift, allowing a smooth interpolation to find the correct opacity for any source redshift and spectral binning. In order to treat the evolution of the EBL photon number density with redshift, a scale factor of 1.7 was introduced (see [13] for a discussion of the scale factor).

- Each observed photon spectrum was corrected for the EBL absorption predicted by each of the generic EBL SEDs, by multiplying each differential flux point in the spectrum by $e^{\tau(E_p,z_s)}$, where the energy corresponds to the energy of the differential flux point and z corresponds to the source redshift.

- A fit is performed for each EBL-deabsorbed spectrum. For sources where the observed spectrum is well-described by a power law, only a power law fit is used. For sources with curved observed spectra, a log parabola and power law with an exponential cutoff are additionally tested when fitting the EBL-deabsorbed spectra. The conditions for the fit to the de-absorbed spectra are the following: the fit model is restricted to be concave for curved fits, and fitted spectral index is bounded to be softer than 1.5. The latter condition is motivated by the expectation the *Fermi*-LAT measured spectrum should provide a good estimate of the intrinsic source spectrum. However, most of the sources show flux variability in both HE and VHE, which has been linked to spectral variability. The less restrictive bound of 1.5 matches the bound observed for *Fermi*-LAT measured flares in [30]. Taking this as the bound removes the uncertainty from possible spectral variability in the HE range.

- At each λ_{EBL}, a histogram is filled with the EBL intensity for EBL SEDs, weighted by $e^{-\chi^2/2}$, where χ^2 is taken from the fit to the de-absorbed spectrum associated to the EBL shape. If multiple fits were performed, the smallest χ^2 is used. The weights from the first step (compensating for non-uniform distribution of intensities) are also applied.

- To combine all sources, the previous step is repeated, weighting by $e^{-\chi^2(tot)/2}$, where $\chi^2(tot)$ is the sum of χ^2 values from all the sources contributing at a given λ_{EBL}. The λ_{EBL} over which a source contributes is determined by the energy range of the source spectrum according to $\lambda_{EBL} = 1.187\ E\ (1+z)^2$ [12].

The final weighted histograms at the fixed λ_{EBL} points give the probability densities for the EBL intensity. In cases where the lower edge of the distribution drops to zero at low EBL intensity, we define the 68% confidence band by finding the 16% containment on the high and low sides of the distribution. Otherwise, we set upper limits by finding the 16% containment on the high side of the distribution.

A closure test was performed by absorbing the spectrum of a nearby source (the Crab Nebula) with the Gilmore 2012 model predictions at several redshifts [5]. Using these test spectra, EBL constraints were derived as described above. The 68% confidence band for the EBL intensity as a function of λ_{EBL} contained the Gilmore 2012 prediction, validating the method.

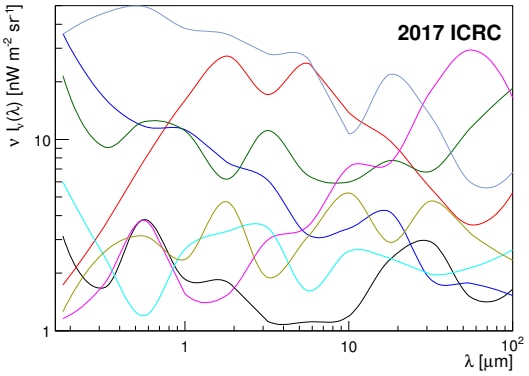

Figure 4: Examples of several generic EBL SED shapes used in the VERITAS EBL analysis.

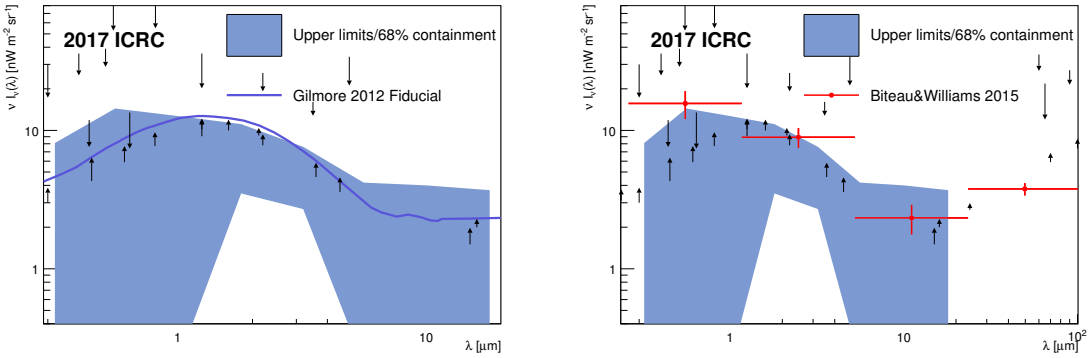

Figure 5: The left panel compares the upper limits on the EBL SED as measured by the VERITAS collaboration against the model of Gilmore 2012. Upper and lower limits from direct measurements and galaxy counts are shown by the upward and downward facing black arrows, respectively. The right panel gives a comparison with previous results.

The derived upper limits on the EBL SED are shown in blue in Fig. 5, interpolated from the containment bands at the fixed λ_{EBL} points. In the left panel, it is compared against the Gilmore 2012 EBL model. In the right panel, it is compared against the results of [13] (using γ-ray data only). Upper and lower limits from direct measurements and galaxy counts are shown by the upward and downward facing black arrows, respectively. The tension with the lower limits from galaxy counts is not significant.

The right panel gives a comparison with previous results. The red points from [13] were derived without including information about galaxy counts, and using a model independent approach starting from generic EBL shapes, and hence can be easily compared to the presented result. A much larger sample of source spectra from the literature were used to produce the plotted points, which accounts for the difference in the uncertainties. No significant tension is observed.

7.2 H.E.S.S.

Preliminary EBL results from the H.E.S.S. collaboration were presented at this conference in

[26] and were shortly thereafter published in [25]. The study utilized observations of the HBLs Mrk 421, Mrk 501, PKS 2005-489, 1ES 0229+200, H 2356-309, 1ES 1101-232, 1ES 0347-121 and 1ES 0414+009, covering a range of redshifts from z=0.031–0.287. Due to flaring activity in Mrk 421 and PKS 2155-304, these datasets were subdivided by flux level, resulting in 21 total spectra from the 8 sources observed. The observed spectra were subjected to a Bayesian unfolding to remove instrumental effects.

The intrinsic source spectra were assumed to have concave log-parabolic shapes (which were allowed to converge to power laws in the case of no curvature). The EBL energy density was broken into energy ranges with the EBL levels ρ_i within the bands. The unfolded spectra were fit with the function $N_0(E/E_0)^{-\alpha-\beta log(E/E_0)}e^{-\tau(-E,\,z,\,\rho_i)}$, with the intrinsic spectral parameters and EBL levels allowed to float.

Comparison to the null hypothesis of no EBL resulted in a 9.5σ detection of the EBL. Systematic uncertainties were assessed, including the EBL evolution with redshift (a minor effect as the most distant blazar in the dataset is at z=0.287), the energy scale uncertainty, and the choice of energy/λ_{EBL} ranges. The resulting EBL SED is shown in Fig. 6, and shows good agreement with lower limits from galaxy counts.

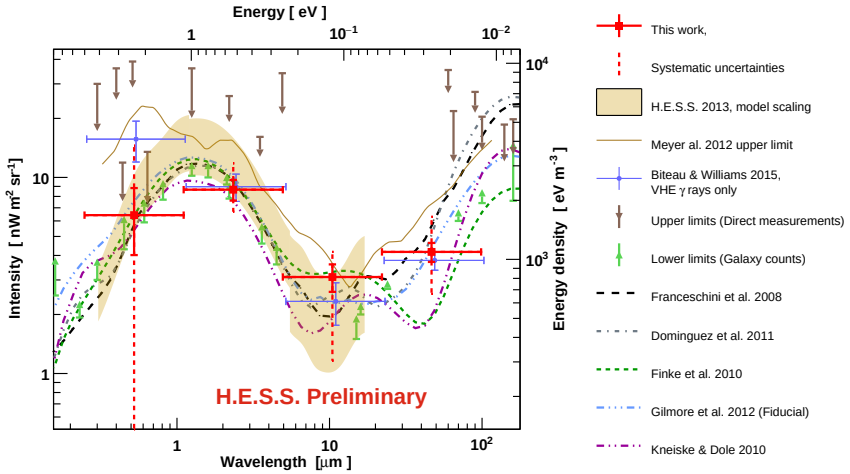

Figure 6: The EBL SED as measured by the H.E.S.S. collaboration. Reproduced from [26].

7.3 MAGIC

The MAGIC collaboration also produced an updated EBL measurement [27], using both a model-dependent approach and a model-independent approach similar to the one used by H.E.S.S. and described above. The measurement used 32 spectra from 12 blazars (Mrk 421, 1ES 1959+650, OT 546, BL Lacertae, 1ES 0229+200, 1ES 1011+496, PKS 1510-089, PKS 1222+216, PG 1553+113, PKS 1424+240, PKS 1441+25 and QSO B0218+35), covering the redshift range z=0.03–0.94. Of the 12 sources, 8 are classified as HBLs, 4 as flat spectrum radio quasars.

The model-dependent approach, presented here, fits the observed spectra with the function $(dN/dE)_{int} \times e^{-\alpha\tau}$, where τ is taken (for the appropriate energy and redshift) from the predictions of [3]. Concave curved spectra were assumed for the intrinsic spectra: power law with exponential

or sub/super exponential cutoff, log parabola, and log parabola with exponential cutoff. Simple power law shapes were not allowed for the intrinsic spectra.

In one case, only the MAGIC-measured spectrum were considered in the fit. In the second, contemporaneous *Fermi*-LAT data were included via a χ^2 penalty for disagreement between the spectral index and flux (at the pivot energy) measured in the *Fermi*-LAT data and the fitted values for the intrinsic MAGIC spectrum. In addition to statistical uncertainties, a systematic uncertainty due to the uncertainty on the energy scale was assessed. The results are shown in Fig. 7 and Fig. 8. Good consistency can be seen between the measurements and lower limits from galaxy counts.

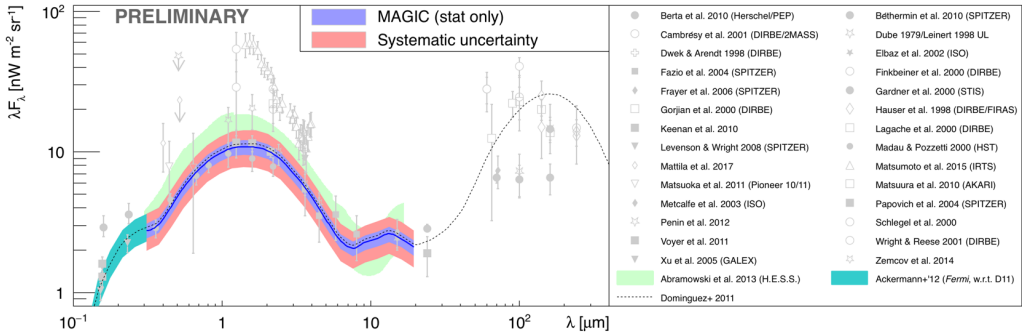

Figure 7: The EBL SED as measured by the MAGIC collaboration, including only VHE spectral information. Reproduced from [27].

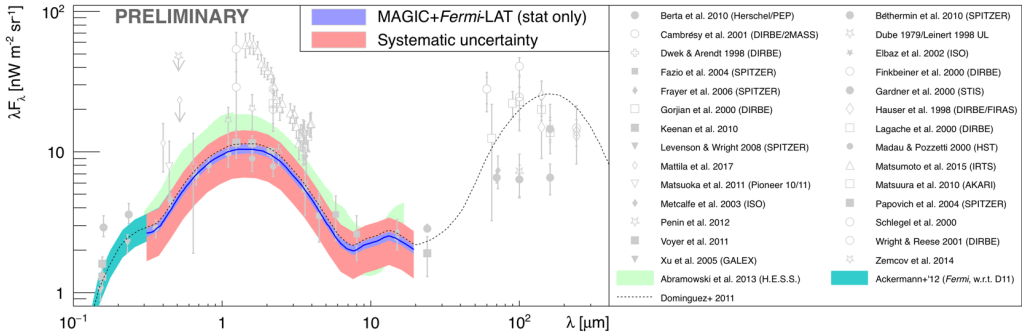

Figure 8: The EBL SED as measured by the MAGIC collaboration, including both VHE and HE spectral information. Reproduced from presentation of [27].

8. Conclusions

Measurement of the extragalactic background light endures as an active area of effort in HE and VHE γ-ray astronomy, due to its significance as a cosmological observable, as well as its importance for interpreting observations of distant γ-ray emitters such as blazars. New results from the IACTs continue to improve our understanding, and show the EBL spectral energy distribution in good agreement with the lower limits derived from galaxy counts. These latest results indicate that additional contributions from exotic processes or a truly diffuse component not associated to

galaxies and stars do not make a large contribution to the total EBL intensity. Further updated measurements from the IACTs and studies with data collected by the upcoming CTA observatory will continue to clarify the picture.

References

[1] Dwek, E. & Krennrich, F. 2013, ApJ, 43, 112

[2] Dole, H. et al. 2006, A&A, 451, 417

[3] Domínguez, A. et al. 2011, MNRAS, 410, 2556

[4] Franceschini, A., Rodighiero, G. & Vaccari, M. 2008, A&A, 487, 837

[5] Gilmore, R.C. et al. 2012, *MNRAS*, 422, 3189

[6] Finke, J.D., Razzaque, S. & Dermer, C.D. 2010, ApJ, 712, 238

[7] Stecker, F.W., Malkan, M.A. & Scully, S.T. 2006, ApJ, 648, 774

[8] Hauser, M.G. & Dwek, E. 2001, Ann. Rev. Astron. Astrophys., 39, 249

[9] Gould, R. J. & Schreder, G. P. 1967, Phys. Rev., 155, 1404

[10] Ackermann, M. et al (*Fermi*–LAT collaboration). 2012, Science, 338, 1190

[11] Mazin, D. & Raue, M. 2017, A&A, 471, 439

[12] Abramowski, A. et al. (H.E.S.S. collaboration). 2013, A&A, 550, A4

[13] Biteau, J. & Williams, D.A. 2015, ApJ, 812, 60

[14] Raue, M. & Mazin, D. 2008, Int. J. Mod. Phys. D, 17, 1515

[15] Atwood, W.B. et al. (*Fermi*–LAT collaboration). 2009, ApJ, 697, 1071

[16] Park, N. et al. (VERITAS collaboration). 2015, PoS(ICRC2015)771

[17] Aleksic, J. et al. (MAGIC collaboration). 2016, Astropart. Phys., 72, 76

[18] Aharonian, F.A. et al. (H.E.S.S. collaboration). 2006, A&A, 457, 899

[19] Ong, R. et al. (CTA collaboration). 2017, Proc. of the 35^{th} ICRC

[20] Ajello, M. et al. (*Fermi*–LAT collaboration). 2017, *accepted by ApJ Supplement*, arXiv:1702.00664

[21] Domínguez, A. & Ajello, M. 2015, ApJ Letters, 813, 2

[22] Domínguez, A. et al. 2013, ApJ, 770, 1

[23] Abeysekara, A.U. et al. (VERITAS collaboration). 2015, ApJ Letters, 815, 2

[24] Gaté, F. et al. (CTA collaboration). 2017, Proc. of the 35^{th} ICRC

[25] Abdalla, H. et al. 2017, *accepted by A&A*, arXiv:1707.06090

[26] Taylor, A. et al (H.E.S.S. collaboration). 2017, Proc. of the 35^{th} ICRC

[27] Moralejo Olaizola, A. et al (MAGIC collaboration). 2017, Proc. of the 35^{th} ICRC

[28] Daniel, M. et al. (VERITAS collaboration). 2007, Proc. of the 30^{th} ICRC

[29] Krause, M., Pueschel, E., & Maier, G. 2017, Astropart. Phys., 89, 1

[30] Abdollahi, S. et. al 2016, *submitted to ApJ Supplement*, arXiv:1612.03165